Ab initio molecular dynamics simulation of photoisomerization in azobenzene in the *n*π* state

Yusuke Ootani,[1] Kiminori Satoh,[1] Akira Nakayama,[1] Takeshi Noro,[1] and Tetsuya Taketsugu[1,2,a)]

[1]*Division of Chemistry, Graduate School of Science, Hokkaido University, Sapporo 060-0810, Japan*
[2]*Department of Theoretical and Computational Molecular Science, Institute for Molecular Science, Okazaki 444-8585, Japan*

Photoisomerization mechanism of azobenzene in the lowest excited state $S_1(n\pi^*)$ is investigated by *ab initio* molecular dynamics (AIMD) simulation with the RATTLE algorithm, based on the state-averaged complete active space self-consistent field method. AIMD simulations show that *cis* to *trans* isomerization occurs via two-step rotation mechanism, accompanying rotations of the central NN part and two phenyl rings, and this process can be classified into two types, namely, clockwise and counterclockwise rotation pathways. On the other hand, *trans* to *cis* isomerization occurs via conventional rotation pathway where two phenyl rings rotate around the NN bond. The quantum yields are calculated to be 0.45 and 0.28 ± 0.14 for *cis* to *trans* and *trans* to *cis* photoisomerizations, respectively, which are in very good agreement with the corresponding experimental results. © *2009 American Institute of Physics*. [doi:10.1063/1.3263918]

I. INTRODUCTION

In the past decade *ab initio* molecular dynamics (AIMD) approach has become one of the standard theoretical methods to examine chemical reaction processes from microscopic viewpoint.[1] AIMD is a classical trajectory method in which atomic positions and velocities are propagated through numerical integration of Newton's equations of motion on the basis of *ab initio* energy gradients, and thus it does not require potential energy functions or potential energy surfaces (PESs) in advance. Examination of minimum energy path on the PES provides a static picture of a given reaction process, while AIMD simulation provides insight into the reaction mechanism from a dynamical viewpoint, and they often help in finding more realistic reaction pathways. Nowadays the applicability of *ab initio* on-the-fly dynamics approach has been extended to photochemical reactions where nonradiative transitions play a significant role.[2–4] In our group, this AIMD method was applied to photochemical reactions in solutions[5,6] and to dissociative recombination reactions with the surface hopping scheme.[7–9] Since the construction of potential energy functions or PESs for electronically excited states is much more difficult than for the ground state, AIMD approach should be a powerful theoretical tool in photochemistry.

Photoisomerization of azobenzene has been extensively studied both experimentally[10–21] and theoretically[22–35] because of its significance as photochromic materials. The *trans* form of azobenzene has a planar structure, whereas in the *cis* form, phenyl rings are twisted around the C–N bonds to minimize steric repulsion, and thus the *cis* form is less stable than the *trans* form. The two isomers can be inter-changed by photoexcitation at suitable wavelengths. The absorption spectra of both *cis*- and *trans*-azobenzenes show a weak band in the visible region and an intense band in the near-UV region, which are attributed to the $n\pi^*$ and $\pi\pi^*$ excitations, respectively.[10–13] For free azobenzene, the quantum yields for isomerization in the $\pi\pi^*$ state (0.09-0.11 for *trans* to *cis* and 0.27-0.42 for *cis* to *trans*) are lower than those in the $n\pi^*$ state (0.23-0.25 for *trans* to *cis* and 0.4-0.56 for *cis* to *trans*) in inert solvents,[14–16] while for sterically hindered azobenzenes, both $n\pi^*$ and $\pi\pi^*$ excitations show almost equal quantum yields.[10,11] Under the assumption that the rotational motion is forbidden in sterically hindered azobenzene, Rau[10,11] proposed that photoisomerization of azobenzene follows different pathways in the $n\pi^*$ and $\pi\pi^*$ states, i.e., NNC inversion and rotation around NN bond, respectively. Their schematic illustrations for inversion and rotation pathways are shown in Fig. 1.

Ultrafast UV-visible absorption spectroscopy and time-resolved fluorescence experiments on *trans*-azobenzene showed[13,17] that the $S_1(n\pi^*)$ decay is described by three processes with lifetimes of 0.30, 2.6, and 12 ps. It was concluded that the first process is the relaxation from the Franck–Condon region to the equilibrium structure in the S_1
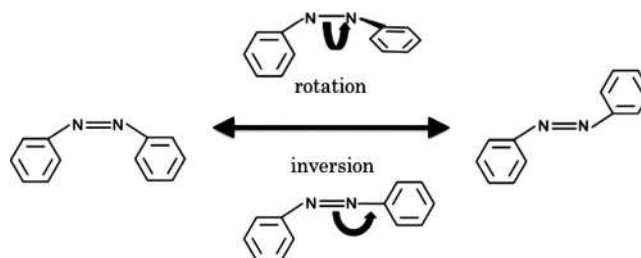

FIG. 1. Schematic structures of inversion and rotation pathways of *cis-trans* photoisomerization reaction of azobenzene.

---

a)Author to whom correspondence should be addressed. Electronic mail: take@sci.hokudai.ac.jp.

state, the second process is the nuclear motion toward S_1/S_0 conical intersections, leading to *trans* or *cis* form of azobenzene, and the third process is the vibrational cooling in the S_0 state through interaction with the solvent. Diau *et al.*[18] examined the anisotropy of the $S_1(n\pi^*)$ fluorescence of *trans*-azobenzene, and proposed that the $S_1(n\pi^*)$ photoisomerization occurs along the NN rotation in hexane while the symmetric inversion pathway is seen in ethylene glycol. Transient absorption experiments for $n\pi^*$ excitation of *cis*-azobenzene showed a fast decay with a dominant component of a time constant of 0.17 ps in ethanol and a weaker component with a time constant of ~ 1 ps.[17] There have been also a number of experimental studies for the $\pi\pi^*$ excitation of *trans*- and *cis*-azobenzenes.[12,13,19–21] Based on the transient Raman and absorption spectra on *trans*-azobenzene, Tahara and co-workers[19–21] proposed that excitation to $S(\pi\pi^*)$ is immediately followed by the decay to $S_1(n\pi^*)$ and that the isomerization paths for the $\pi\pi^*$ and $n\pi^*$ excitations are the same, which should be the inversion pathway.

The first theoretical calculations on photoisomerization of azobenzene were reported by Monti *et al.*[22] in 1982. They performed small configuration interaction calculations using the STO-3G basis set for the ground and excited states at four geometries, i.e., the *trans* and *cis* isomers, and activated complexes along the rotation and inversion pathways. The calculated potential energy curves of S_1 show a large barrier for the rotation pathway while the inversion pathway has no barrier, and thus they concluded that the isomerization through S_1 is likely to proceed via an inversion pathway. This picture had been adopted in many experiments for a long time. In 1999, Cattaneo and Persico[23] performed complete active space self-consistent field (CASSCF) and multireference perturbation calculations (CASPT2) for this photoisomerization, and suggested that the inversion is the preferred pathway for the ground state isomerization, and that such inversion probably occurs via $n\pi^*$ excitation, while rotation occurs by $\pi\pi^*$ excitation. In 2001, Ishikawa *et al.*[24] constructed the two-dimensional PES of $S_1(n\pi^*)$ as a function of the CNNC torsion and NNC bond angles, and showed that S_1/S_0 conical intersection exists near the midpoint of the rotation pathway. Based on the calculated PES, they first proposed that the rotation pathway is the preferred one in the $S_1(n\pi^*)$ state. After this theoretical report, a number of theoretical calculations were performed on the reaction pathways for photoisomerization of azobenzene on the $S_1(n\pi^*)$ surface by CASSCF, CASPT2, and time-dependent (TD) density functional theory (DFT) methods, which all support the rotation mechanism for the $S_1(n\pi^*)$ photoisomerization.[25–28] The on-the-fly dynamics simulations based on semiempirical molecular orbital calculations were also performed by the surface hopping method[29,31,33] and by the multiple spawning method,[30] both of which support that the rotation mechanism is the preferred pathway. Very recently several dynamics simulations have also been performed to examine mechanism of photoisomerization of azobenzene at the DFT level,[34,35] but there has been no report on *ab initio* dynamics simulations of this photoreaction including nonadiabatic transitions.

In this study we perform AIMD simulations for *cis* to *trans* and *trans* to *cis* photoisomerizations of azobenzene in the $S_1(n\pi^*)$ state at the CASSCF level. In AIMD approach, all nuclear degrees of freedom are automatically included, indicating that a relatively small time step is required to describe the fast motions such as X-H stretching vibrations in a molecule. If such fast motions are not significant in a given reaction, a relatively large time step can be employed by fixing those internal degrees of freedom through dynamics simulation. Such methodology was developed in a conventional molecular dynamics framework, named as SHAKE[36] and RATTLE.[37] In this work, we implement the RATTLE algorithm to our developed surface hopping AIMD code, and examine the dynamics of *cis-trans* photoisomerization process of azobenzene by AIMD simulations with geometrical constraint on CH bond lengths in phenyl rings.

In Sec. II, we briefly describe the excited-state AIMD methodology as well as the RATTLE algorithm. Descriptions of computational details are followed, and then we discuss the results of AIMD simulations, including the reaction pathways, the lifetime of the S_1 decay, and the quantum yields of photoisomerization.

II. EXCITED-STATE AIMD METHOD WITH INTERNAL CONSTRAINT

We have developed an AIMD program code for excited-state dynamics with Tully's surface hopping scheme,[38] in which nuclear coordinates are propagated by integrating Newton's equations of motion, based on *ab initio* energy gradients, while electronic wave function is propagated by integrating the TD Schrödinger equation using nonadiabatic coupling terms. For a given time t, the electronic wave function ψ is expanded in terms of adiabatic eigenfunctions, $\{\phi_\nu\}$, as

$$\psi(\mathbf{r};\mathbf{R}(t)) = \sum_\nu c_\nu(t)\phi_\nu(\mathbf{r};\mathbf{R}(t)), \qquad (1)$$

where $c_\nu(t)$ denotes the electronic amplitude, and $\mathbf{r}$ and $\mathbf{R}(t)$ denote electronic and nuclear coordinates, respectively. Substituting Eq. (1) into the TD Schrödinger equation,

$$i\hbar\frac{\partial\psi}{\partial t} = \hat{H}\psi, \qquad (2)$$

we obtain a time-evolution equation for electronic amplitudes as

$$i\hbar\dot{c}_\mu = c_\mu V_\mu - i\hbar\sum_\nu c_\nu\dot{\mathbf{R}}\cdot\mathbf{d}_{\mu\nu}, \qquad (3)$$

where V_μ and $\mathbf{d}_{\mu\nu}$ denote the μth adiabatic energy and nonadiabatic coupling terms between μth and νth adiabatic states, respectively. The electronic amplitudes $\{c_\mu\}$ are developed by numerical integration of Eq. (3) along the trajectory. Following Tully's fewest switches algorithm,[38] the probability of surface hopping from the μth to the νth electronic adiabatic states within the time of $t\sim t+\Delta t$ is evaluated from the electronic amplitudes and nonadiabatic coupling terms as

$$P_{\mu\nu}(t) = -2\frac{\mathrm{Re}(\dot{\boldsymbol{R}}\cdot\boldsymbol{d}_{\mu\nu})c_\mu c_\nu^*}{|c_\mu|^2}\Delta t. \tag{4}$$

The surface hopping is invoked when $P_{\mu\nu}(t)$ becomes greater than a uniform random number generated between 0 and 1.

In the above scheme, energy gradients and nonadiabatic coupling terms are evaluated by *ab initio* electronic structure calculations at each step, and thus, it requires a large number of *ab initio* calculations, leading to an enormous computational cost. In order to reduce the computational cost, we introduce the internal constraint for fast but insignificant motions, which enables us to employ a relatively large time step. RATTLE[37] was developed in a scheme of the velocity-Verlet algorithm, in which the constraint force is introduced in Newton's equations of motion as

$$m_i\ddot{\boldsymbol{R}}_i = \boldsymbol{F}_i + \boldsymbol{G}_i, \tag{5}$$

where m_i and $\boldsymbol{R}_i$ denote the ith atomic mass and position coordinates, respectively, and $\boldsymbol{F}_i$ and $\boldsymbol{G}_i$ denote a Born–Oppenheimer force and a constrained force acting on the ith atom, respectively. The constrained condition for an interatomic distance between the ith and jth atoms is written as

$$|\boldsymbol{R}_i(t) - \boldsymbol{R}_j(t)|^2 - l_{ij}^2 = 0, \tag{6}$$

where l_{ij} is a fixed interatomic distance. The constrained condition for velocity can be obtained through the derivative of Eq. (6) with respect to time as

$$\{\dot{\boldsymbol{R}}_i(t) - \dot{\boldsymbol{R}}_j(t)\}\cdot\{\boldsymbol{R}_i(t) - \boldsymbol{R}_j(t)\} = 0. \tag{7}$$

The constrained force $\boldsymbol{G}_i$ is determined so that the atomic positions $\boldsymbol{R}_i$ and velocity $\dot{\boldsymbol{R}}_i$ satisfy the constraint conditions Eqs. (6) and (7) in an iterative manner.

III. COMPUTATIONAL DETAILS

We have carried out AIMD simulations for *cis-trans* photoisomerization of azobenzene in the lowest excited state $S_1(n\pi^*)$ at the state-averaged CASSCF (SA-CASSCF) level. In SA-CASSCF calculations, five electronic states, S_0, $S_1(n\pi^*)$, $S_2(n\pi^*)$, $S_3(n^2\pi^{*2})$, and $S_4(\pi\pi^*)$, were included with the same weight, and the active space was composed of six electrons in four orbitals (n,n,π,π^*). Analytical energy gradients and nonadiabatic coupling terms were calculated by solving coupled-perturbed multiconfiguration SCF equations. As the basis set, STO-3G has been utilized. All electronic structure calculations were performed by the MOL-PRO2006 program package.[39]

In AIMD simulations, RATTLE algorithms were applied to solve Newton's equations of motion with geometrical constraint that all CH bond lengths in two phenyl rings were fixed to the equilibrium distances in the S_0 state. In order to examine the applicability of the RATTLE algorithm, we performed preliminary AIMD simulations, starting from *cis* form of azobenzene, on the S_1 state with and without internal constraint by using several time steps, 0.3, 0.6, 0.9, and 1.2 fs. With each time step, ten trajectories were calculated for 90 fs, and then the numerical errors in total energy and geometrical parameters were examined. As the reference trajectory, we also calculated an AIMD trajectory by the velocity-

TABLE I. $n\pi^*$ excitation energies ΔE (eV) and optimized geometries in the ground state calculated with STO-3G and TK/NOSeC-V-DZP. Bond length r is given in Å and bond angle a and dihedral angle d are given in degrees.

		STO-3G	DZP	Expt.
cis	ΔE	3.78	3.46	2.85[a]
	r_{NN}	1.266	1.213	1.253[b]
	r_{CN}	1.490/1.490	1.440/1.440	1.449[b]
	a_{NNC}	120.5/120.5	122.9/122.9	121.9[b]
	d_{CNNC}	3.4	4.3	8.0[b]
	d_{NNCC}	65.1/65.1	62.5/62.5	53.3[b]
trans	ΔE	2.96	3.24	2.75[c]
	r_{NN}	1.277	1.215	1.247[d]
	r_{CN}	1.476/1.476	1.429/1.429	1.428[d]
	a_{NNC}	112.0/112.0	114.9/114.9	114.1[d]
	d_{CNNC}	180.0	180.0	180.0[d]
	d_{NNCC}	0.0/0.0	0.0/0.0	0.0[d]

[a]Reference 17.
[b]Reference 41.
[c]Reference 20.
[d]Reference 42.

Verlet algorithm (no geometry constraint) with a time step of 0.1 fs. Following preliminary calculations, we performed AIMD simulations starting from *cis* or *trans* structure, with a time step of 1.0 fs. For nonadiabatic region, however, a short time step, 0.1 fs, was employed to reduce numerical errors in integration of time-evolution equations for nuclei and electronic wave functions. In total, 200 trajectories have been run starting from *cis*-azobenzene up to 240 fs, while 100 trajectories have been run starting from *trans*-azobenzene up to 3 ps. The initial condition for atomic positions and velocities were determined by the canonical sampling (T=300 K) using normal modes of vibration in the ground state of azobenzene.

IV. RESULTS AND DISCUSSION

A. Preliminary calculations

In order to discuss quantum yields of *cis-trans* photoisomerization of azobenzene from AIMD simulations, a large number of trajectories are required, and thus we should make an effort to reduce the computational cost as much as possible. The most expensive part of AIMD simulations lies in *ab initio* electronic structure calculations. In this work, we employ the SA-CASSCF method with the small basis set, STO-3G, to save the computational time. To check the accuracy of this basis set, we calculated equilibrium structures of *cis*- and *trans*-azobenzenes and $n\pi^*$ excitation energies by the Hartree–Fock and SA-CASSCF methods, respectively, with two different basis sets, STO-3G and TK/NOSeC-V-DZP (double-zeta-plus-polarization quality, although polarization functions for C and H are omitted).[40] The results are summarized in Table I. As a general tendency, the excitation energies are overestimated, compared to the corresponding experimental values.[17,20] On the other hand, optimized geometries are almost in good agreement with the experimental ones,[41,42] although the NNCC dihedral angle for *cis*-azobenzene is ~10° larger than the experimental value.
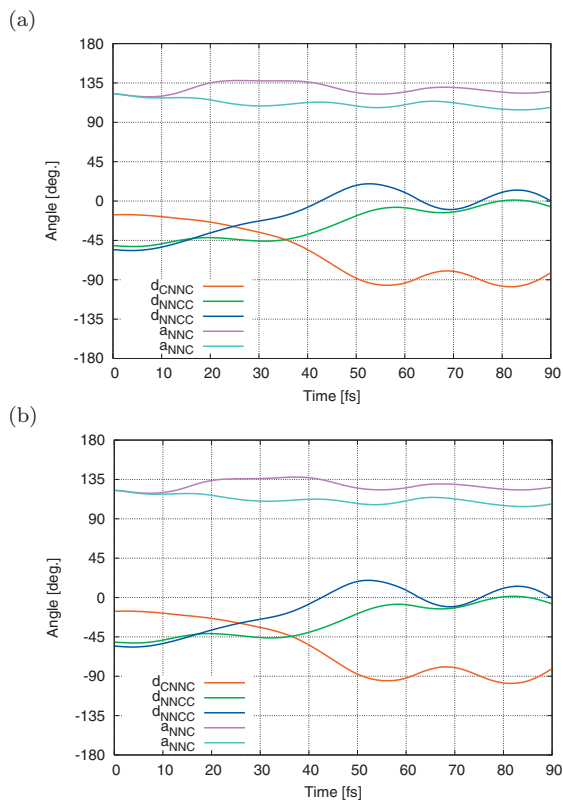
(a)

(b)

FIG. 2. Variations of selected geometrical parameters along the trajectory starting from the same initial condition, calculated by (a) the velocity-Verlet algorithm with 0.1 fs step and (b) the RATTLE algorithm with 1.2 fs step.

FIG. 3. An absolute error in total energy per femtosecond averaged over 90 fs.

We also examined potential energy curves along NNC bond angle (a_{NNC}), CNNC dihedral angle (d_{CNNC}), and NNCC dihedral angle (d_{NNCC}) in the S_0 and S_1 states, and verified that potential energy curves calculated with STO-3G qualitatively reproduce those calculated with TK/NOSeC-V-DZP at the CASSCF level. For *cis* to *trans* photochemical channel, the energy variation of the S_1 state along d_{CNNC} shows a barrierless feature, while for *trans* to *cis* photochemical channel, the corresponding energy variation shows an almost flat feature near the Franck–Condon region ($d_{CNNC} = 180° - 165°$) at the SA-CASSCF level with STO-3G and TK/NOSeC-V-DZP basis set. This region is very important for dynamics from *trans* to *cis* isomerization, and so we also performed multireference second-order perturbation theory (RS2C) calculations with TK/NOSeC-V-DZP basis set to determine the potential energy curve along d_{CNNC} and confirmed that the RS2C potential energy curve shows the same feature as the SA-CASSCF one. Based on the results of preliminary calculations, we decided to employ the SA-CASSCF method with STO-3G basis sets for the following AIMD simulations.

An alternative idea to reduce the computational costs in AIMD simulations is the reduction in the number of points at which *ab initio* calculations are performed. For this purpose we employ the RATTLE algorithm in integrating Newton's equations of motion, by which insignificant degrees of freedom are fixed throughout the simulations. It is noted that by this constraint, one does not need to worry about zero-point vibrational motions related to these degrees of freedom. Fig-
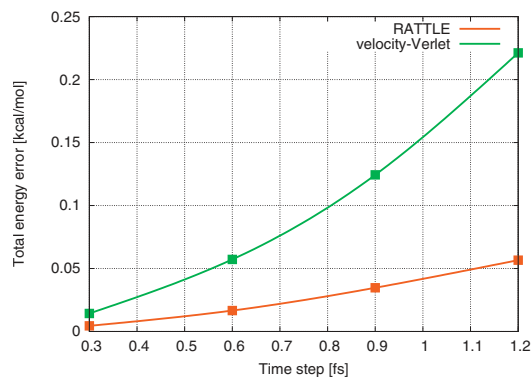
ure 2 shows variations of selected geometrical parameters along the trajectory starting from the same initial condition, calculated by (a) the velocity-Verlet algorithm with 0.1 fs step and (b) the RATTLE algorithm with 1.2 fs step. For the sake of the comparison, the surface hopping is not invoked throughout the simulation. As is shown here, these two graphs look almost identical, indicating that geometry constraints for CH bond lengths introduce no serious error in reaction pathway. Figure 3 shows an absolute error in total energy per femtosecond averaged over 90 fs, as a function of the time step length. The error in no-constrained trajectories is three to four times larger than the one in constrained trajectories, suggesting that the constraint for CH vibrational motion enables one to employ the larger time step. We also examined effects of time step length on the time evolution of electronic amplitudes with a surface hopping algorithm turned on. Figure 4 shows variations of the norm of the respective electronic adiabatic states as a function of time derived by three different conditions: (a) velocity-Verlet with 0.1 fs step (reference), (b) RATTLE with 1.2 fs step, and (c) RATTLE with hybrid steps of 1.2+0.1 fs. In these simulations, the same set of random number was employed in decision of the surface hopping. In this trajectory, the molecule reaches the nonadiabatic regions of S_0 and S_1 around $t = 47$ fs, where a rapid change in electronic amplitudes is shown. In a case of Fig. 4(b), however, surface hopping does not occur at this nonadiabatic region, and the molecule stays on S_1 until $t \sim 60$ fs. This result is clearly incorrect, which is caused by numerical error in integrating of the TD Schrödinger equation for electronic amplitudes. In order to ensure the accuracy of numerical integration, we attempted to employ the shorter time step, 0.1 fs, only at the nonadiabatic region where an energy difference between S_0 and S_1 becomes less than 10 kcal/mol (in other words, hybrid time steps, 1.2 and 0.1 fs, are employed for adiabatic and nonadiabatic regions, respectively). Then we observe the correct behavior in variations of electronic amplitudes, as shown in Fig. 4(c). It is concluded that as long as a short time step is employed at the nonadiabatic region, geometry constraint for CH bond lengths allows us to employ the larger time step.

B. AIMD simulations

Following the preliminary calculations described above, we have run 200 trajectories starting from *cis* form of
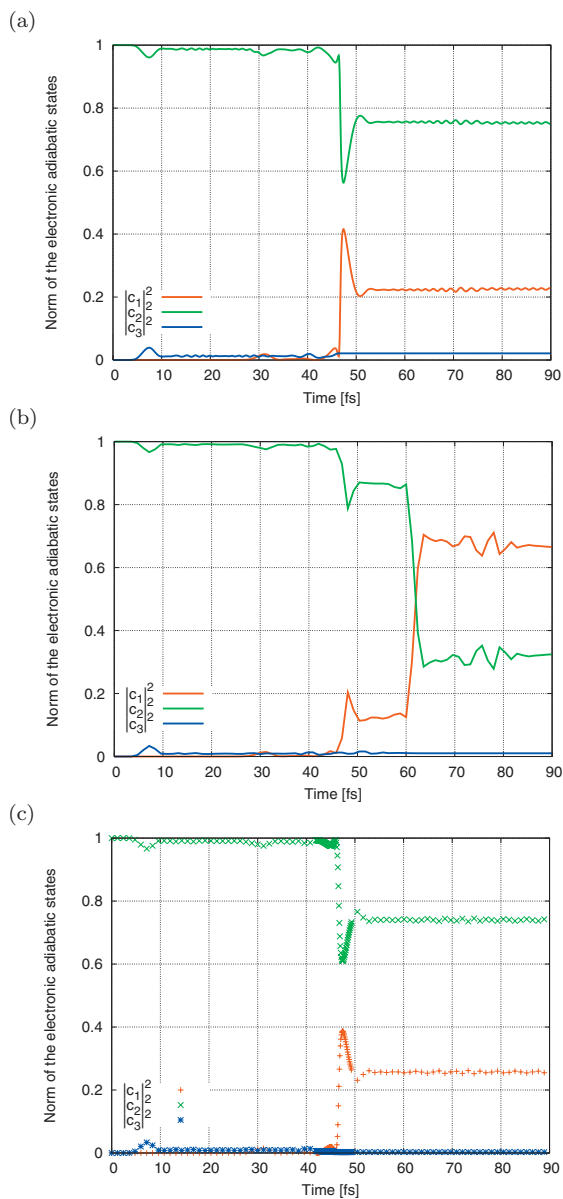
(a)

(b)

(c)

FIG. 4. Variations of the norm of the respective electronic adiabatic states as a function of time derived by three different conditions: (a) velocity-Verlet with 0.1 fs step, (b) RATTLE with 1.2 fs step, and (c) RATTLE with hybrid steps of 1.2 fs+0.1 fs.

(i) Clockwise rotation

$t = 0.0$
$d_{CNNC} = 2.9$
$d_{NNCC} = -71.9/-68.1$

$t = 43.2$
$d_{CNNC} = 92.2$
$d_{NNCC} = -132.6/-92.4$

$t = 240.3$
$d_{CNNC} = 170.9$
$d_{NNCC} = 114.1/-49.4$

(ii) Counterclockwise rotation

$t = 0.0$
$d_{CNNC} = -21.0$
$d_{NNCC} = -49.7/-43.6$

$t = 38.9$
$d_{CNNC} = -86.0$
$d_{NNCC} = -0.7/8.2$

$t = 240.2$
$d_{CNNC} = 165.0$
$d_{NNCC} = -41.7/77.2$

(iii) Counterclockwise (S_1) + Clockwise (S_0) rotation

$t = 0.0$
$d_{CNNC} = -6.0$
$d_{NNCC} = -54.6/-56.3$

$t = 39.4$
$d_{CNNC} = -85.7$
$d_{NNCC} = -12.1/13.1$

$t = 169.4$
$d_{CNNC} = 1.0$
$d_{NNCC} = -91.3/-49.3$

$t = 215.4$
$d_{CNNC} = 90.2$
$d_{NNCC} = -147.9/-114.7$

$t = 240.4$
$d_{CNNC} = 151.0$
$d_{NNCC} = -155.3/-128.1$

FIG. 5. Snapshots along example trajectories for (i) clockwise rotation, (ii) counterclockwise rotation, and (iii) counterclockwise (S_1)+clockwise (S_0) rotation, starting from *cis*-azobenzene.

azobenzene up to 240 fs by employing the RATTLE algorithm. Among 200 trajectories, isomerization to *trans*-azobenzene occurs in 90 trajectories while the remaining 110 trajectories go back to the region of *cis*-azobenzene in the ground state, and thus, the quantum yield for *cis* to *trans* photoisomerization is estimated to be 0.45. For reactive trajectories, the reaction pathway can be classified into three patterns, as shown in Fig. 5: (i) clockwise rotation, (ii) counterclockwise rotation, and (iii) counterclockwise (S_1) +clockwise (S_0) rotation. In the respective patterns, the second snapshot corresponds to the structure at which the surface hopping to S_0 occurs. As shown in these snapshots, only the central N–N part moves drastically in the initial 40 fs while two phenyl rings do not move so much from the initial position because of the difference in masses between N atoms and phen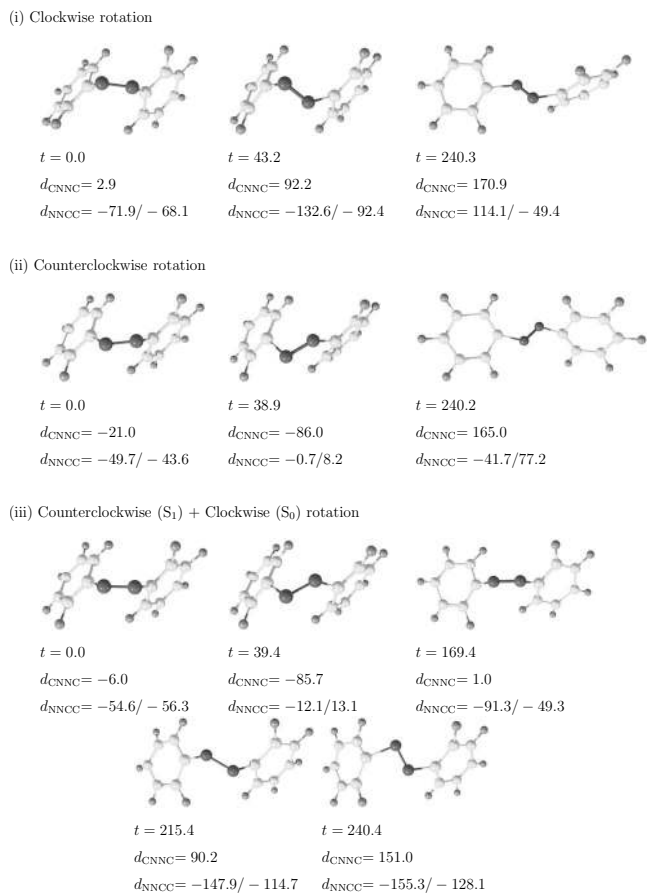yl rings. The rotational direction of the N–N part is clockwise in the first pathway while it is counterclockwise in the second and third pathways. After the CNNC dihedral angle d_{CNNC} reaches $\sim 90°$ or $-90°$, corresponding to the midpoint between *cis*- and *trans*-form structures, surface hopping to S_0 occurs and both phenyl rings start to move toward a structure of *trans*-azobenzene, completing the isomerization. In the first and second pathways two phenyl rings keep their moving directions after hopping to S_0, while in the third pathway they turn about on the S_0 surface [this pathway is referred to as counterclockwise (S_1)+clockwise (S_0) rotation]. Atomic motions along the AIMD trajectory do not correspond to the conventional rotation pathway where two phenyl rings rotate around the central NN bond. In the simple picture of rotation mechanism a structural transformation accompanies a movement of two heavy phenyl rings in a long distance (rotation with a large moment of inertia), while in the pathway presented here, the rotation proceeds in two steps, i.e., (1) rotation of the central N–N part and (2) rotation of two phenyl rings with much shorter distance. Because two phenyl rings are deviated from the central C–N–N–C plane in *cis*-azobenzene, the initial rotation of NN part makes molecular structure close to the S_1/S_0 minimum energy conical intersection (MECI) point (which will be discussed later) without a movement of phenyl rings. Then two phenyl rings rotate about the C–N bond, resulting in the structure of *cis* or *trans* form of azobenzene in the S_0 state.

Figure 6 shows variations of selected geometrical pa-

(i) Clockwise

(ii) Counterclockwise

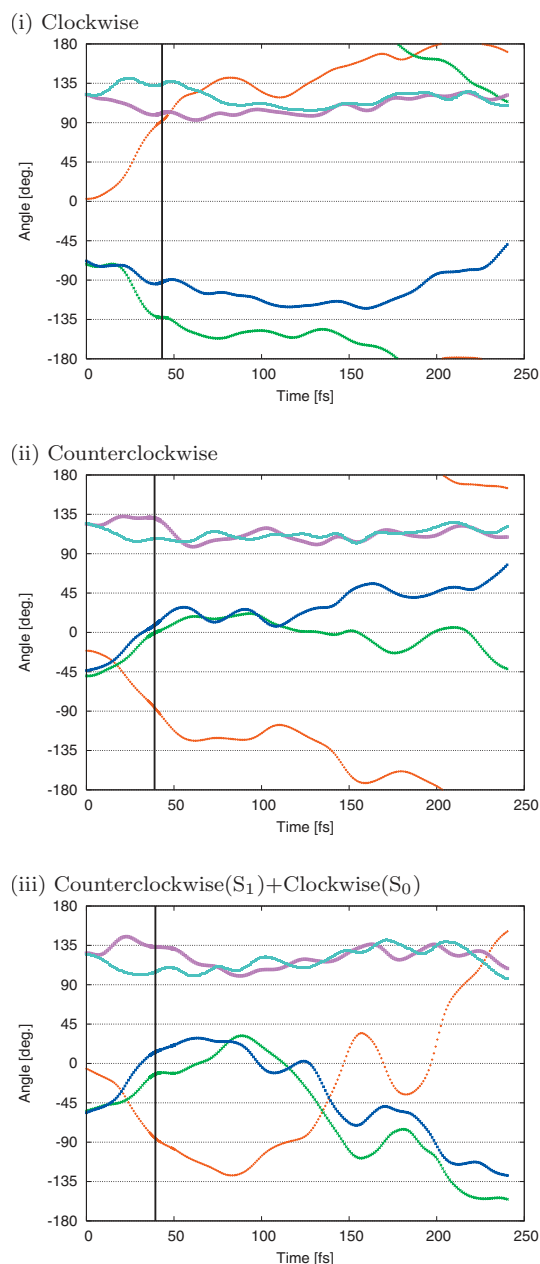(iii) Counterclockwise(S_1)+Clockwise(S_0)

FIG. 6. Variations of selected geometrical parameters, namely, NNC bond angles, NNCC dihedral angles, and CNNC dihedral angle, along the trajectories given in Fig. 5. Light blue and pink marks denote NNC bond angles, blue and green marks denote NNCC dihedral angles, and red mark denotes CNNC dihedral angle. Vertical solid line denotes the surface hopping time.

rameters, namely, NNC bond angles, NNCC dihedral angles, and CNNC dihedral angle, along the trajectories given in Fig. 5. Starting from the $S_1(n\pi^*)$ state, surface hopping to the S_0 state occurs at $t=43.2$, 38.9, and 39.4 fs in Figs. 6(a)–6(c), respectively, which are denoted by the vertical solid line. In the initial stage before hopping to S_0, one NNC bond angle increases to 140° while the other decreases to 100°, and then they show fluctuations around the respective positions, indicating that this is not the inversion pathway. On the other hand, the CNNC dihedral angle immediately increases or decreases, and reaches to 90° or −90°, where surface hopping occurs. This feature indicates that the reaction proceeds along the rotation pathway, but as discussed

above, this is not a conventional rotation pathway. It is interesting to note that both NNCC dihedral angles show twist motions in the direction opposite to change in the CNNC dihedral angle. The numbers of trajectories classified to the respective patterns are counted as 13, 64, and 13 for the clockwise rotation, counterclockwise rotation, and counterclockwise (S_1)+clockwise (S_0) rotation, respectively, and thus counterclockwise rotation is the most preferred pathway. Actually we also performed the steepest-descent-path calculations in mass-weighted Cartesian coordinates, starting from the Franck–Condon *cis* structure, on the S_1 surface, and found that it is the counterclockwise rotation pathway. It is noteworthy that through AIMD simulations we have found a new pathway, i.e., clockwise rotation pathway. In some trajectories, surface hopping occurs from S_0 to S_1, but the molecule immediately goes back to S_0. As to unreactive trajectories, either clockwise or counterclockwise rotational motion proceeds in the initial stage, and then the molecule goes back to the region of *cis*-azobenzene.

Here we turn to analyses of AIMD trajectories starting from *trans* form of azobenzene. As was described in Sec. I, the reaction rate for *trans*-azobenzene is much slower than that for *cis*-azobenzene because the *trans*- and *cis*-azobenzenes have planar and nonplanar equilibrium structures, respectively, and so it takes much longer time for *trans*-azobenzene to deviate from the planar structure. Taking into account the reaction rate, we have run 100 trajectories starting from *trans* form of azobenzene with the time length of 3 ps, although trajectory calculation is stopped when the molecule reaches the region of *trans* or *cis* form in the S_0 state. As the results of AIMD simulations, isomerization to *cis*-azobenzene occurs in 24 trajectories, while in 62 trajectories, the molecule goes back to the region of *trans*-azobenzene in the ground state. The remaining 14 trajectories continue to stay in the S_1 state during the simulation time of 3 ps. Thus, the quantum yield for *trans* to *cis* photoisomerization is estimated as 0.28 ± 0.14. Figure 7 shows snapshots for examples of two reactive [(i) and (ii)] and unreactive (iii) trajectories. It is noted that clockwise and counterclockwise rotation pathways are essentially identical with each other in *trans*-azobenzene. In the respective trajectories, the second snapshot corresponds to the structure at which the surface hopping to S_0 occurs. Compared to the reaction pathway in *cis* to *trans* isomerization, atomic movements along the trajectory show a conventional rotation pathway where two phenyl rings rotate around the NN bond. Figure 8 shows variations of selected geometrical parameters, NNC bond angles, NNCC dihedral angles, and CNNC dihedral angle, along the trajectories given in Fig. 7. Both NNC bond angle oscillates around 120°, and NNCC dihedral angles show fluctuations with out of phase to each other. For the reactive trajectory, surface hopping to S_0 occurs at $t=800–900$ fs, and then CNNC dihedral angle starts to change drastically and the molecule transforms from *trans* to *cis* structure very quickly (within 50 fs). On the S_1 surface, NN bond length shows fluctuations around the equilibrium bond length in S_1, 1.367 Å, which is ~0.1 Å larger than the equilibrium distance of 1.277 Å in S_0. This feature is due to the character of electronic structure of $S_1(n\pi^*)$, where the NN bond order is
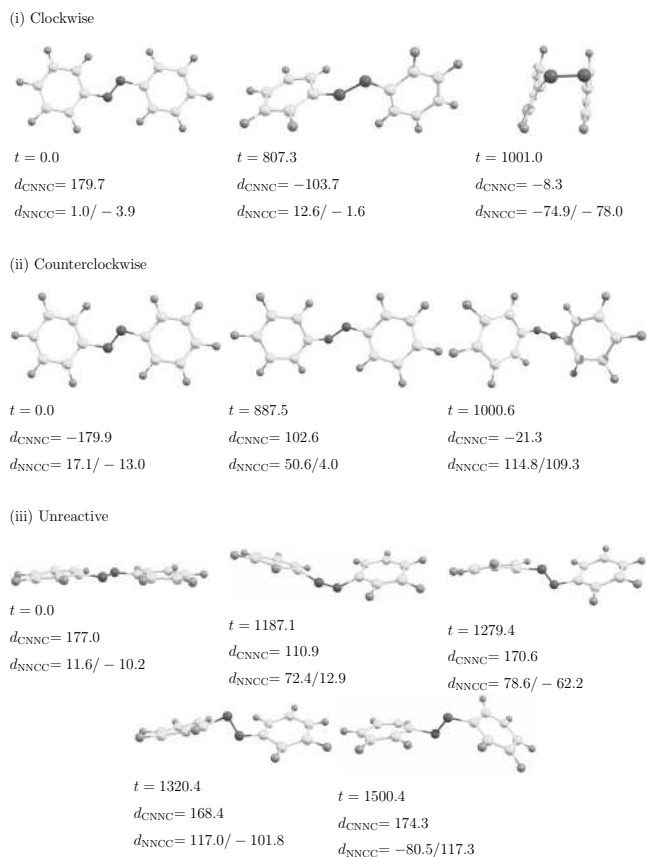
(i) Clockwise

$t = 0.0$
$d_{CNNC} = 179.7$
$d_{NNCC} = 1.0 / -3.9$

$t = 807.3$
$d_{CNNC} = -103.7$
$d_{NNCC} = 12.6 / -1.6$

$t = 1001.0$
$d_{CNNC} = -8.3$
$d_{NNCC} = -74.9 / -78.0$

(ii) Counterclockwise

$t = 0.0$
$d_{CNNC} = -179.9$
$d_{NNCC} = 17.1 / -13.0$

$t = 887.5$
$d_{CNNC} = 102.6$
$d_{NNCC} = 50.6 / 4.0$

$t = 1000.6$
$d_{CNNC} = -21.3$
$d_{NNCC} = 114.8 / 109.3$

(iii) Unreactive

$t = 0.0$
$d_{CNNC} = 177.0$
$d_{NNCC} = 11.6 / -10.2$

$t = 1187.1$
$d_{CNNC} = 110.9$
$d_{NNCC} = 72.4 / 12.9$

$t = 1279.4$
$d_{CNNC} = 170.6$
$d_{NNCC} = 78.6 / -62.2$

$t = 1320.4$
$d_{CNNC} = 168.4$
$d_{NNCC} = 117.0 / -101.8$

$t = 1500.4$
$d_{CNNC} = 174.3$
$d_{NNCC} = -80.5 / 117.3$

FIG. 7. Snapshots along example trajectories for (i) clockwise rotation, (ii) counterclockwise rotation, and (iii) unreactive trajectories, starting from *trans*-azobenzene.

~1.5. For the unreactive trajectory, both NNCC dihedral angles show violent fluctuations but they do not correspond to the rotational motion of phenyl rings. Both phenyl rings keep their positions, while the central N atoms show a bicycle-pedal motion, which is illustrated in Fig. 7(iii).

C. Analyses of reaction mechanism

In order to provide insight into the reaction pathway of photoisomerization of azobenzene, we have constructed two-dimensional PESs of S_0 and S_1 states as a function of CNNC and NNCC dihedral angles where two NNCC dihedral angles are fixed to the same value, and all other degrees of freedom are fixed to those of the equilibrium structure of *cis*-azobenzene in the ground state. Figure 9 shows the calculated PESs for (a) S_0 and (b) S_1 states. In this two-dimensional coordinate space, two points which are symmetric with respect to the origin correspond to enantiomer to each other. In the S_0 surface there is an energy barrier between *trans* and *cis* minima, while in the S_1 surface, the *cis* structure is located at the high energy region. The S_1/S_0 crossing seam locates at the position in the middle value of CNNC dihedral angle, and the MECI is located at $d_{CNNC} \simeq -96.0°$ and $d_{NNCC} \simeq -5.2°$ and $-2.4°$. Figure 10 shows traces of example trajectories, shown in Figs. 5 and 7, projected onto the two-dimensional coordinate space defined above for (a) those starting from *cis* form and (b) those starting from *trans* form. In the former case, the trajectory immediately

(i) Clockwise

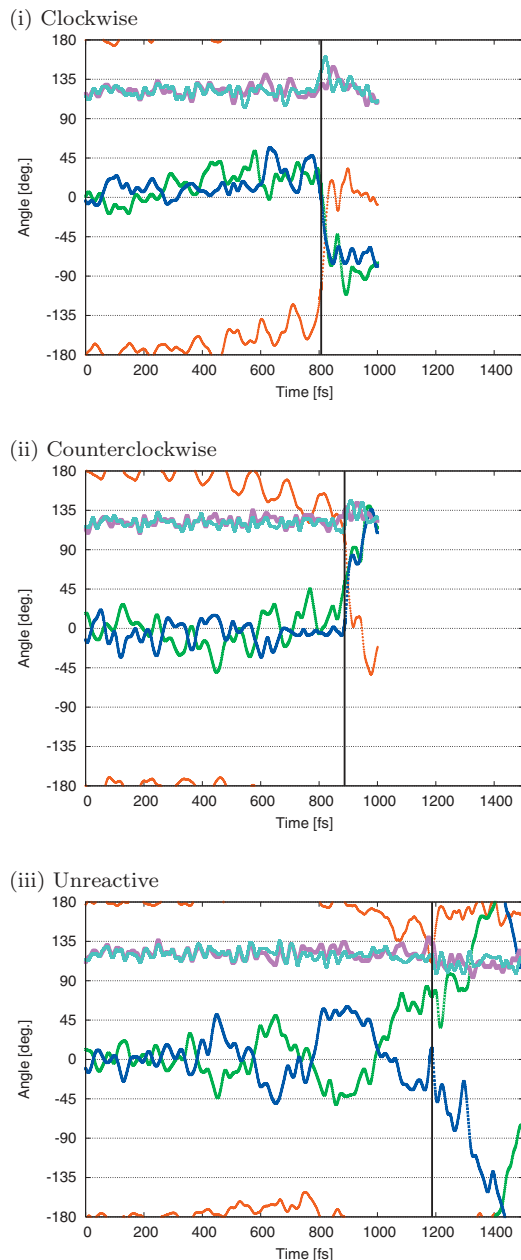(ii) Counterclockwise

(iii) Unreactive

FIG. 8. Variations of selected geometrical parameters, namely, NNC bond angles, NNCC dihedral angles, and CNNC dihedral angle, along the trajectories given in Fig. 7. Light blue and pink marks denote NNC bond angles, blue and green marks denote NNCC dihedral angles, and red mark denotes CNNC dihedral angle. Vertical solid line denotes the surface hopping time.

proceeds to the S_1/S_0 crossing seam since the *cis* structure is located in the high energy region. In the latter case, the trajectory stays around the *trans* structure for much longer time because of the shallow minimum of the PES around there. From a dynamical viewpoint, the structural transformation can be invoked when some amount of energy come together with the reaction coordinate of CNNC dihedral angle, which makes it possible to escape from the shallow well of *trans*-form planar structure in the S_1 state.

Figure 11 shows variations of S_1 population averaged over 200 trajectories (starting from *cis* form) and over 100
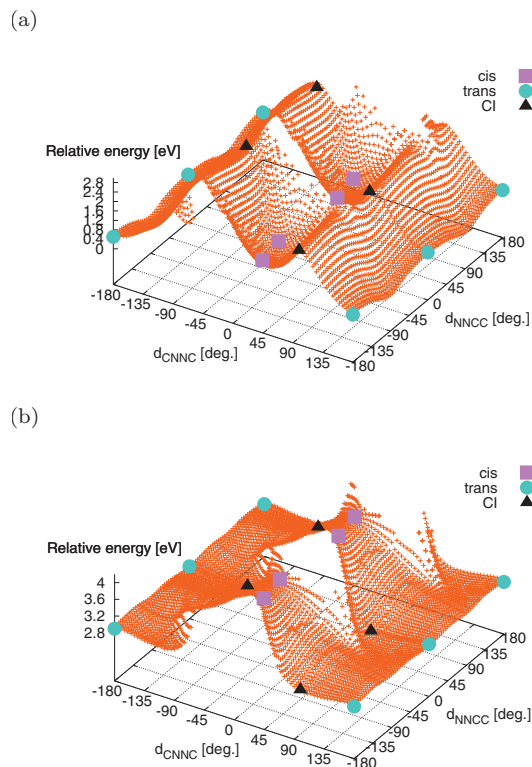
(a)

(b)

FIG. 9. PES as a function of CNNC and NNCC dihedral angles for (a) S_0 and (b) S_1 states.
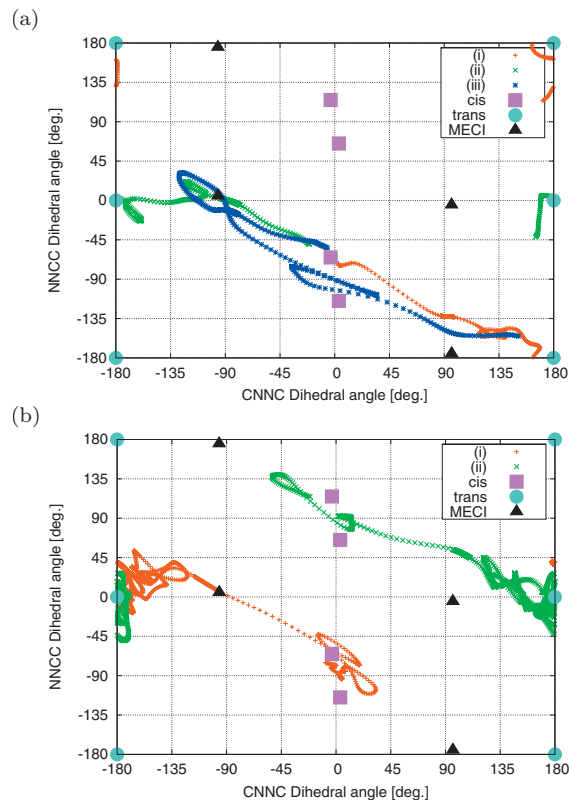
(a)

(b)

FIG. 10. Example trajectories projected onto the two-dimensional coordinate space, (a) starting from *cis* form and (b) starting from *trans* form.

trajectories (starting from *trans* form) as a function of time. By fitting these curves to an exponential function, the lifetimes of S_1 for *cis*- and *trans*-azobenzenes are evaluated as 0.06 and 1.86 ps, respectively. These values are in qualitative agreement with the experimental lifetimes, 0.17 and 2.6 ps, respectively.[13,17]

In our simulations, the quantum yield for *cis* to *trans* photoisomerization is calculated to be 0.45, which is almost twice as large as that for *trans* to *cis* photoisomerization, 0.28 ± 0.14. In order to understand what determines the branching of products further, we examine distributions of CNNC dihedral angle and its velocity at the surface hopping time in Fig. 12 [(a) starting from *cis* form and (b) starting from *trans* form]. The CNNC dihedral angle is 0° and ±180° at *cis* and *trans* structures, respectively, and the S_1/S_0 MECI (MECI$_{S_1/S_0}$) locates at $d_{CNNC} \sim \pm 96°$. In trajectories starting from *cis* form, surface hopping occurs in a very narrow region close to MECI$_{S_1/S_0}$, while in those starting from *trans* form, surface hopping occurs in a wide region between *trans* structure and MECI$_{S_1/S_0}$. In Fig. 12(a), points with $d_{CNNC} = -90°$ correspond to trajectories classified to the counterclockwise rotation pathway, while points with $d_{CNNC} = 90°$ correspond to those for the clockwise rotation pathway. Reactive trajectories show the same sign in d_{CNNC} and its velocity, i.e., negative velocity for $d_{CNNC} \sim -90°$ while positive velocity for $d_{CNNC} \sim 90°$, which is a reasonable feature from a dynamical viewpoint. In contrast to this, for AIMD simulations starting from *trans* form [Fig. 12(b)], reactive trajectories show the different signs in d_{CNNC} and its velocity, i.e., negative velocity for $d_{CNNC} \sim 90°$ while positive velocity for $d_{CNNC} \sim -90°$. In both cases, there is no tendency in a sign of

velocity for d_{CNNC} in unreactive trajectories. Table II summarizes the surface hopping time, t_{hop}, and d_{CNNC} and a velocity for d_{CNNC} at t_{hop}, averaged over the respective reactive and unreactive trajectories which are initiated from *cis* form of azobenzene. Actually unreactive trajectories show almost zero velocity in average (0.33 and 0.36 deg/fs for counterclockwise and clockwise rotation, respectively). It is also noted that the velocity of d_{CNNC} for counterclockwise (S_1) + clockwise (S_0) rotation has a negative value [blue dots in Fig. 12(a)]. In these trajectories, the NN part turns its direction from counterclockwise to clockwise on the S_0 surface, and goes toward the *trans* structure with d_{CNNC} increasing to 180°. As shown in Table II, this type of trajectory shows the earliest surface hopping time and the largest velocity of
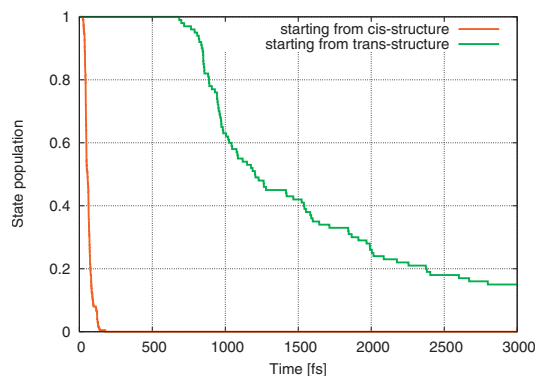

FIG. 11. Variations of S_1 population averaged over 200 trajectories (starting from *cis* form) and over 100 trajectories (starting from *trans* form) as a function of time.
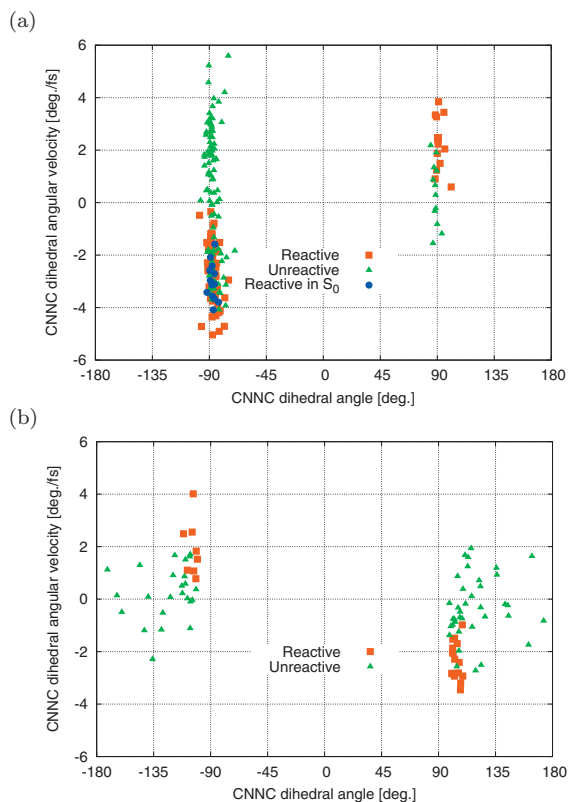
(a)

(b)

FIG. 12. The distribution of CNNC dihedral angle and its velocity at the surface hopping time for trajectories (a) starting from *cis* form and (b) starting from *trans* form.

d_{CNNC}, indicating that they hop to the S_0 state with less energy distributions over other internal degrees of freedom. Therefore, d_{CNNC} reaches the maximum value much earlier than others and turns its direction to increase, reaches to the region of *trans* form ($d_{CNNC} \sim 180°$) over the *cis* region ($d_{CNNC} \sim 0°$). This process may be difficult if much energy is distributed over various degrees of freedom.

Table III summarizes calculated and experimental quantum yields for photoisomerization of azobenzene. Our results, 0.45 and 0.28 ± 0.14 for *cis* to *trans* and *trans* to *cis*, respectively, are in very good agreement with the experimental results, although our simulation is performed for isolated molecule while the experimental results are obtained in solution. We confirmed that our calculated quantum yields almost converge with respect to the number of trajectories. The previous theoretical results overestimated the experimental values, which may be attributed to the use of semiempirical molecular orbital calculations. In future work we will per-

TABLE II. Averaged surface hopping time, t_{hop}, and CNNC dihedral angle and its velocity at t_{hop} for trajectories initiated from *cis* form of azobenzene.

	t_{hop} (fs)	d_{CNNC} (deg)	$\dot{d}_{CNNC}$ (deg/fs)
Unreactive counterclockwise	58.1	−87.0	0.33
Unreactive clockwise	72.1	88.5	0.36
Reactive counterclockwise	64.0	−87.1	−2.56
Reactive clockwise	76.7	91.8	2.24
Counterclockwise (S_1)+clockwise (S_0)	47.3	−87.4	−3.01

TABLE III. Calculated and experimental quantum yields for isomerization.

	AIMD[a]	SH[b]	FMS[c]	Expt.[d]
cis to *trans*	0.45	0.61 ± 0.03	0.68 ± 0.11	0.40–0.56
trans to *cis*	0.28 ± 0.14	0.33 ± 0.03	0.46 ± 0.08	0.23–0.25

[a]Our calculated results.
[b]Surface hopping results taken from Ref. 30.
[c]Full multiple spawning results taken from Ref. 30.
[d]Experimental results taken from Refs. 14–16.

form AIMD simulations with increasing number of trajectories, employing more correlated method and the better basis sets in the electronic structure calculations, and also including the solvent effects explicitly.

V. CONCLUSION

AIMD approaches are now widely used in a variety of chemical processes including photochemical reactions. Statistical analyses of AIMD simulations require a large number of trajectories accompanying a large number of *ab initio* electronic structure calculations, and thus it is very important to make efforts to reduce the computational costs in both *ab initio* calculations and MD simulations. In the present work, we implemented the RATTLE algorithm in our AIMD code which can exclude insignificant degrees of freedom from full-dimensional AIMD simulations. When these constrained degrees of freedom are the fastest ones, one can employ the larger time step for integration of Newton's equations of motion. Also, one can use this code to examine the significance of the respective degrees of freedom by comparing RATTLE-AIMD simulations with full-dimensional AIMD simulations.

We applied the RATTLE-AIMD approach to *cis-trans* photoisomerization reactions of azobenzene at the SA-CASSCF level in order to examine the reaction pathway as well as the quantum yields for isomerization. Through preliminary test calculations, we decided to employ the time step of 1.0 fs for AIMD simulations, although, in a nonadiabatic region, a short time step of 0.1 fs was employed. In total, 200 trajectories have been run, starting from *cis* form, while 100 trajectories have been run, starting from *trans* form. The reaction mechanism is basically classified into rotation pathway in both reactions. In trajectories starting from *cis* form, the central NN bond rotates initially in counterclockwise or clockwise way while two phenyl rings stay at almost the initial positions due to differences in masses of N atoms and phenyl rings. Since two phenyl rings are deviated from the central C–N–N–C plane at the equilibrium structure, the initial rotation of central NN bond makes the molecular configuration close to the MECI point with $d_{CNNC} \sim 90°$, and surface hopping to S_0 occurs very quickly ($t \sim 50$ fs). On the other hand, in trajectories starting from *trans* form, the molecule stays at the initial planar structure for a relatively long time, and surface hopping to S_0 occurs around $t \sim 800$ fs. The quantum yields for isomerization are calculated as 0.45 and 0.28 ± 0.14 for *cis* to *trans* and *trans* to *cis* isomerizations, respectively, which are in very good agreement with the experimental values.

ACKNOWLEDGMENTS

[1] M. S. Gordon, G. Chaban, and T. Taketsugu, J. Phys. Chem. **100**, 11512 (1996).

[2] T. Vreven, F. Bernardi, M. Garavelli, M. Olivucci, M. A. Robb, and H. B. Schlegel, J. Am. Chem. Soc. **119**, 12687 (1997).

[3] A. L. Kaledin and K. Morokuma, J. Chem. Phys. **113**, 5750 (2000).

[4] M. Ben-Nun, J. Quenneville, and T. J. Martinez, J. Phys. Chem. A **104**, 5161 (2000).

[5] D. Kina, A. Nakayama, T. Noro, T. Taketsugu, and M. S. Gordon, J. Phys. Chem. A **112**, 9675 (2008).

[6] D. Kina, P. Arora, A. Nakayama, T. Noro, M. S. Gordon, and T. Taketsugu, Int. J. Quantum Chem. **109**, 2308 (2009).

[7] T. Taketsugu, A. Tajima, K. Ishii, and T. Hirano, Astrophys. J. **608**, 323 (2004).

[8] M. Kayanuma, T. Taketsugu, and K. Ishii, Chem. Phys. Lett. **418**, 511 (2006).

[9] M. Kayanuma, T. Taketsugu, and K. Ishii, Theor. Chem. Acc. **120**, 191 (2008).

[10] H. Rau and E. Lüddeke, J. Am. Chem. Soc. **104**, 1616 (1982).

[11] H. Rau, in *Photochromism: Molecules and Systems*, edited by H. Dürr and H. Bounas-Laurent (Elsevier, Amsterdam, 1990), Vol. 1, Chap. 4, pp. 165–192.

[12] I. K. Lednev, T.-Q. Ye, R. E. Hester, and J. N. Moore, J. Phys. Chem. **100**, 13338 (1996).

[13] I. K. Lednev, T.-Q. Ye, P. Matousek, M. Towrie, P. Foggi, F. V. R. Neuwahl, S. Umapathy, R. E. Hester, and J. N. Moore, Chem. Phys. Lett. **290**, 68 (1998).

[14] P. Bortolus and S. Monti, J. Phys. Chem. **83**, 648 (1979).

[15] G. Zimmerman, L.-Y. Chow, and U.-J. Paik, J. Am. Chem. Soc. **80**, 3528 (1958).

[16] D. Gegiou, K. A. Muszkat, and E. Fisher, J. Am. Chem. Soc. **90**, 12 (1968).

[17] T. Nägele, R. Hoche, W. Zinth, and J. Wachtveitl, Chem. Phys. Lett. **272**, 489 (1997).

[18] C.-W. Chang, Y.-C. Lu, T.-T. Wang, and E. W.-G. Diau, J. Am. Chem. Soc. **126**, 10109 (2004).

[19] T. Fujino and T. Tahara, J. Phys. Chem. A **104**, 4203 (2000).

[20] T. Fujino, S. Y. Arzhantsev, and T. Tahara, J. Phys. Chem. A **105**, 8123 (2001).

[21] T. Fujino, S. Y. Arzhantsev, and T. Tahara, Bull. Chem. Soc. Jpn. **75**, 1031 (2002).

[22] S. Monti, G. Orlandi, and P. Palmieri, Chem. Phys. **71**, 87 (1982).

[23] P. Cattaneo and M. Persico, Phys. Chem. Chem. Phys. **1**, 4739 (1999).

[24] T. Ishikawa, T. Noro, and T. Shoda, J. Chem. Phys. **115**, 7503 (2001).

[25] A. Cembran, F. Bernardi, M. Garavelli, L. Gagliardi, and G. Orlandi, J. Am. Chem. Soc. **126**, 3234 (2004).

[26] E. W.-G. Diau, J. Phys. Chem. A **108**, 950 (2004).

[27] M. L. Tiago, S. Ismail-Beigi, and S. G. Louie, J. Chem. Phys. **122**, 094311 (2005).

[28] I. Conti, M. Garavelli, and G. Orlandi, J. Am. Chem. Soc. **130**, 5216 (2008).

[29] C. Ciminelli, G. Granucci, and M. Persico, Chem.-Eur. J. **10**, 2327 (2004).

[30] A. Toniolo, C. Ciminelli, M. Persico, and T. J. Martinez, J. Chem. Phys. **123**, 234308 (2005).

[31] C. Ciminelli, G. Granucci, and M. Persico, J. Chem. Phys. **123**, 174317 (2005).

[32] C. Nonnenberg, H. Gaub, and I. Frank, ChemPhysChem **7**, 1455 (2006).

[33] G. Granucci and M. Persico, Theor. Chem. Acc. **117**, 1131 (2007).

[34] J. Shao, Y. Lei, Z. Wen, Y. Dou, and Z. Wang, J. Chem. Phys. **129**, 164111 (2008).

[35] P. Sauer and R. E. Allen, Chem. Phys. Lett. **450**, 192 (2008).

[36] J.-P. Ryckaert, G. Ciccotti, and H. J. C. Berendsen, J. Comput. Phys. **23**, 327 (1977).

[37] H. C. Andersen, J. Comput. Phys. **52**, 24 (1983).

[38] J. C. Tully, J. Chem. Phys. **93**, 1061 (1990).

[39] MOLPRO, a package of *ab initio* programs written by H.-J. Werner and P. J. Knowles, version 2006.1, R. D. Amos, A. Bernhardsson, A. Berning *et al.*

[40] See: http://setani.sci.hokudai.ac.jp/sapporo/.

[41] A. Mostad and C. Romming, Acta Chem. Scand. (1947-1973) **25**, 3561 (1971).

[42] J. A. Bouwstra, A. Schouten, and J. Kroon, Acta Crystallogr., Sect. C: Cryst. Struct. Commun. **39**, 1121 (1983).